Thermo-magnetic loading effects on high-frequency dynamic behaviour of magnetic shape memory alloys

Emmanuel Omotosho, Zhuofan Qin, Martin Birkett, Xue Chen, Ben Bin Xu*
Faculty of Engineering and Environment, Northumbria University, Newcastle upon Tyne, NE1 8ST, UK

Abstract

This paper theoretically studies the thermo-magnetic loading effects on the long-term (> 100 s, reaching the steady state) high-frequency (> 100 Hz) dynamic behaviour of magnetic shape memory alloys actuated by cyclic magnetic fields. The material's dynamic behaviour at different levels of ambient heat-transfer, ambient temperature, applied magnetic field frequency and amplitude are simulated by a dynamic model incorporating both magnetic-field-induced martensite reorientation and temperature-driven martensitic phase transformation. Analytical expressions of the material's long-term steady-state behaviour (i.e., stable strain amplitude and temperature) as a function of ambient thermal conditions and magnetic loading conditions are further derived. It is found from model simulations and analytical calculations that weak ambient heat-transfer, high ambient temperature, and high magnetic field amplitude (to trigger martensite reorientation) lead to large net heat generation from dissipative martensite reorientation and thus increase material's stable temperature, which results in reduced twinning stress and increased stable strain amplitude. It is also found that the material's stable temperature can reach the characteristic phase transformation temperature triggering the martensite-to-austenite transformation. In this case, weaker ambient heat transfer, higher ambient temperature and higher magnetic field frequency result in larger heat generation rate accelerating the martensite-to-austenite transformation. Therefore, less martensite remains in the material and the material's stable strain amplitude becomes smaller.

Keywords: magnetic shape memory alloys, high-frequency magnetic actuation, martensite reorientation, martensitic transformation, ambient thermal effect, magnetic loading effect

*Corresponding author.
Tel.: +44 (0)191 227 3608; Email address: ben.xu@northumbria.ac.uk (B. B. Xu).

1. Introduction

Magnetic shape memory alloys (MSMAs) are a kind of magneto-active materials (Bastola and Hossain, 2021a, 2021b; Lucarni et al., 2022; Yarali et al., 2022). Large strain up to 10% can be achieved due to martensitic phase transformation or martensite reorientation (Bruno et al., 2016; Haldar and Lagoudas, 2018; Pagounis et al., 2014; Seiner et al., 2014; Sratong-on et al., 2019; Uchimali and Vedantam, 2021; Yu et al., 2018). The main advantage of MSMAs over traditional shape memory alloys is their high-frequency (> 100 Hz) magnetic-field-induced strain, which makes them promising candidates for large-stroke quick-response actuators in the future (Asua et al., 2014; Chernenko et al., 2019; Hobza et al., 2018; Lindquist and Müllner, 2015; Song et al., 2013; Yin et al., 2016).

Ni-Mn-Ga single crystal is the most studied MSMAs. It exhibits three variants in the state of five-layered modulated martensite (Tickle et al., 1999; Webster et al., 1984; Zasimchuk et al., 1990): M1, M2, and M3 with their short axis along the *x*, *y*, and *z*-coordinate, respectively, as shown in Fig. 1(a). Phase transformation between austenite and martensite and martensite reorientation (i.e., switching between different martensite variants) can be induced by thermo-magneto-mechanical loadings, leading to a macroscopic strain change in the material (see Fig. 1(b)).

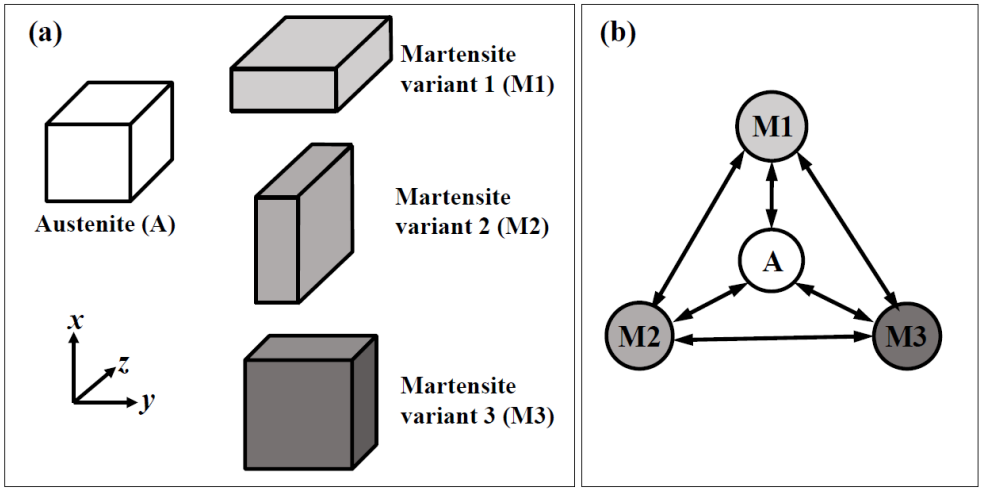

Fig. 1. (a) Schematic diagram of the austenite and the martensite variants of Ni-Mn-Ga magnetic shape memory alloy: cubic austenite lattice and pseudo-tetragonal martensite lattice. (b) Martensite reorientation among three martensite variants (M1, M2, M3) and phase transformation between austenite (A) and martensite (M).

The promising application of MSMAs as fast magnetic actuators has led to several experimental studies on the dynamic behaviour of magnetic-field-induced martensite reorientation in Ni-Mn-Ga single crystal (Faran and Shilo, 2015; Haldar and Lagoudas, 2018; Henry et al., 2002; Karaca et al., 2006; Lindquist and Müllner, 2015; Pascan et al., 2015). Henry (2002) studied the MSMAs' output strain at magnetic field frequencies ranging from 1 Hz to 250 Hz and found a strain decrease when the frequency reached a threshold. Such strain decrease was due to the weakening of the applied magnetic field when the frequency increased. Lai et al. (2008) studied the twin boundary motion in MSMAs at frequencies up to 600 Hz and discovered that the twin-boundary velocity was not the limiting factor in the actuation performance of MSMAs. Techapiesancharoenkil et al. (2009, 2011) experimentally demonstrated the relationship between magnetic field and output strain in dynamic Ni-Mn-Ga actuators. Recent experiments in (Zhang et al., 2018a, 2018b; Zhang et al., 2020) focused on long-term (> 100 s) dynamic behaviour of MSMAs, revealed a new phenomenon: the accumulated heat from the intrinsic dissipation of the cyclic martensite reorientation induced by cyclic magnetic field can significantly increase the material's temperature. Under the weak ambient heat-transfer condition, the phase transformation temperature can be reached, and the martensite-to-austenite transformation can be triggered, leading to a sudden strain drop of the material.

Besides the effect of the ambient heat transfer condition, other loading factors such as ambient temperature, applied magnetic field frequency and amplitude may also influence the dynamic behaviour of MSMAs. Studies on the effect of magnetic field frequency in the literature (e.g., Henry, 2002; Lai et al., 2008; Techapiesancharoenkil et al., 2009) are only focused on a short period of time and those on the effect of magnetic field amplitude (e.g., Karaca et al., 2006; Xie, 2022) are in the quasi-static case. The long-term (> 100 s, reaching the steady state) high-frequency (> 100 Hz) dynamic behaviour of MSMAs is essential for the actuator applications since it is closely related to the reliability and service lifetime of the actuator. Thus, studies of various effects on the long-term high-frequency dynamic behaviour of MSMAs are highly desired, especially the loading factors, which can be used to modulate the actuator's performance. Unfortunately, to the authors' best knowledge, systematic studies on the effects of thermo-magnetic loading factors in the long-term high-frequency dynamic behaviour of MSMAs are seldom reported in the literature.

In this paper, we extend our previous work (Chen and He, 2020) to theoretically study the ambient thermal effects of ambient temperature and ambient heat-transfer condition, and the magnetic loading effects of magnetic field frequency and amplitude on the long-term (>

100 s) high-frequency (> 100 Hz) dynamic behaviour of MSMAs actuated by cyclic magnetic fields. Besides numerical simulations using a mass-spring-damper model incorporating martensite reorientation and martensitic phase transformation of MSMAs, theoretical analysis is also conducted to derive analytical expressions of material's steady-state behaviours (i.e., stable output strain amplitude and temperature) as a function of ambient thermal conditions and magnetic loading conditions. The role played by each thermo-magnetic loading factor is revealed from model simulations and theoretical analysis.

Table 1. Nomenclature

a_0	Magnetic susceptibility of austenite	6×10^2 (Heczko, 2005)		S	Cross-sectional area of MSMAs sample	6 (Zhang et al., 2018b)	mm^2
a_1	Magnetic susceptibility of martensite variant 1	0.95 (Heczko, 2005)		T	MSMAs sample's temperature		°C
a_2	Magnetic susceptibility of martensite variant 2	5×10^2 (Heczko, 2005)		T_0	Ambient temperature	−20 ~ 50	°C
A_s^0	Austenite start temperature in free state	41.5 (Zhang et al., 2018b)	°C	T_{PT}	Characteristic phase transformation temperature	39	°C
c	Damping coefficient	10.1	$kg \cdot s^{-1}$	t_h	Characteristic heat relaxation time	0.1 ~ 1000	s
c_0	Internal energy difference between austenite and martensite at 0 K	1.0768×10^7	$J \cdot m^{-3}$	z_0	Volume fraction of austenite	Initial value $z_0^{(0)} = 0$	
c_1	Entropy difference between austenite and martensite at 0 K	3.4534×10^4	$J \cdot m^{-3} \cdot K^{-1}$	z_1	Volume fraction of martensite variant 1	Initial value $z_1^{(0)} = 1$	
E	Young's modulus of MSMAs sample	50 from mechanical test in (Chen et al., 2013)	GPa	z_2	Volume fraction of martensite variant 2	Initial value $z_2^{(0)} = 0$	
f_H	Applied magnetic field frequency	50 ~ 150	Hz	z_{01}	volume-fraction transformation between austenite and martensite variant 1	Initial value of 0	
k	Interaction parameter accounting for incompatibility among martensite variants	1.09×10^3	$J \cdot m^{-3}$	z_{02}	volume-fraction transformation between austenite and martensite variant 2	Initial value of 0	
k_0	Interaction parameter accounting for incompatibility	2.3810×10^4	$J \cdot m^{-3}$	z_{12}	volume-fraction transformation between	Initial value of 0	

	between austenite and martensite				martensite variant 1 and 2		
k_s	Spring stiffness	5.5 from tests in (Zhang et al., 2018a)	N · mm^{-1}	ε_0	Strain change due to martensite reorientation	5.8% (Heczko, 2005)	
L	Linear coefficient	1×10^4	m · s · kg^{-1}	ε_a	Strain change along long axis of pseudo-tetragonal martensite during martensitic phase transformation	1.9% (Heczko et al., 2002)	
l_0	Initial length of MSMAs sample	15 (Zhang et al., 2018a)	mm	ε_c	Strain change along short axis of pseudo-tetragonal martensite during martensitic phase transformation	3.9% (Heczko, 2002)	
m	Mass of the moving parts in MSMAs dynamic system	22.5 from tests in (Zhang et al., 2018a)	g	λ	Specific heat per unit volume	4×10^6 (Zhang et al., 2018a)	J · m^{-3} · K^{-1}
M_s^A	Saturation magnetization of austenite	3.9×10^5 (Heczko, 2005)	A · m^{-1}	μ_0	Vacuum permeability	$4\pi \times 10^{-7}$	T · m · A^{-1}
M_s^M	Saturation magnetization of martensite	5×10^5 (Heczko, 2005)	A · m^{-1}	$\mu_0 H_{amp}^{app}$	Amplitude of applied magnetic field	0 ~ 1	T
N	Demagnetization factor	0.55 (calculated using the formula in (Aharoni, 1998))		σ_0	Initial compressive stress	0.4 (Zhang et al., 2018a)	MPa
R	Effective radius of MSMAs sample	1.2 (Zhang et al., 2018b)	mm	σ_{tw}^{eff}	Effective twinning stress of martensite reorientation		Pa

2. Dynamic model

A schematic diagram of the MSMAs-based magnetic actuator is shown in Fig. 2(a). The compressive stress along *x*-axis is applied by a spring and the magnetic field along *y*-axis is applied by a pair of electromagnets. Airflow at different temperatures and velocities passes through the sample surface to control the ambient thermal condition. The MSMAs sample is in the initial state of martensite. During the magnetic actuation (i.e., cyclic magnetic field), cyclic martensite reorientation between the stress-preferred variant (M1) and the magnetic-field-preferred variant (M2) is induced in the sample (see inset of Fig. 2(b)), which leads to the cyclic

strain output. Depending on the thermo-magnetic loading conditions, martensite-to-austenite phase transformation may also be induced, as shown in the inset of Fig. 2(b).

The mass-spring-damper model in Fig. 2(b) is used to describe the dynamic behaviour of the MSMAs sample in Fig. 2(a). The material model for the martensite reorientation and martensitic phase transformation of MSMAs developed in (Chen et al., 2014; Chen and He, 2020) is embedded into the mass-spring-damper model. The governing equations covering thermo-magneto-mechanical analyses are summarized below. Detailed deductions of these equations can be found in (Chen and He, 2020).

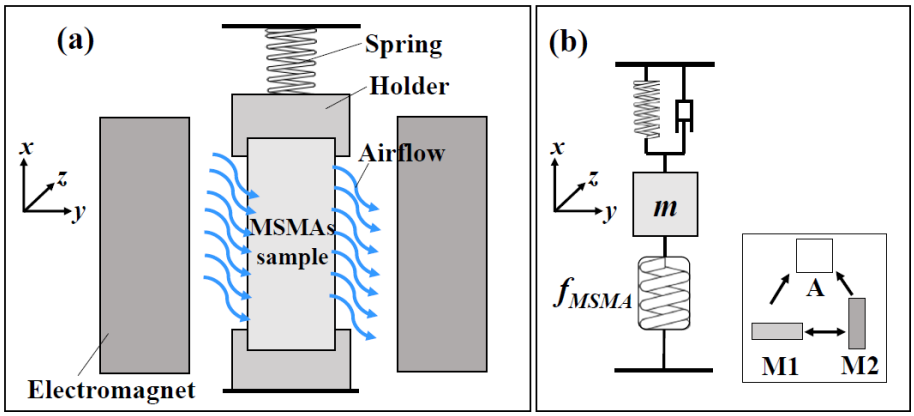

Fig. 2. (a) Schematic diagram of loading conditions for MSMAs-based magnetic actuator. (b) Mass-spring-damper model of the dynamic MSMAs system. f_{MSMA} is the restoring force provided by the MSMAs sample itself. Cyclic martensite reorientation between variant 1 (M1) and 2 (M2) is induced during the magnetic actuation. Martensite-to-austenite (A) phase transformation may also be induced, depending on the thermo-magnetic loading conditions.

- Magnetic analysis

The internal magnetic field H (only considering y-component) in the MSMAs sample can be estimated as:

$$H = H^{app} - N(z_0 M_0 + z_1 M_1 + z_2 M_2) \quad (1)$$

where H^{app} is the magnetic field applied by the electromagnets, N is the demagnetization factor, z_0, z_1 and z_2 are the volume fraction of austenite, and martensite variant 1 and 2, respectively (denoted by A, M1 and M2 in the inset of Fig. 2(b)), and M_0, M_1, M_2 are their respective magnetizations:

$$M_0 = \begin{cases} -M_S^A & \left(H < -\frac{M_S^A}{a_0}\right) \\ a_0 H & \left(-\frac{M_S^A}{a_0} \le H \le \frac{M_S^A}{a_0}\right) \\ M_S^A & \left(H > \frac{M_S^A}{a_0}\right) \end{cases} \quad M_i = \begin{cases} -M_S^M & \left(H < -\frac{M_S^M}{a_i}\right) \\ a_i H & \left(-\frac{M_S^M}{a_i} \le H \le \frac{M_S^M}{a_i}\right) \\ M_S^M & \left(H > \frac{M_S^M}{a_i}\right) \end{cases} \quad (i = 1, 2) \quad (2)$$

with M_S^A and M_S^M being the saturation magnetization of austenite and martensite, respectively, and a_0 and a_i (i = 1, 2) being the magnetic susceptibility of austenite and martensite variant i, respectively.

- Mechanical analysis

Cyclic martensite reorientation between M1 and M2 is induced during the magnetic actuation. The thermodynamic force $A_{1\leftrightarrow 2}$ for martensite reorientation between M1 and M2 can be calculated as (Chen and He, 2020):

$$A_{1\leftrightarrow 2} = \frac{E\varepsilon_0}{l_0}x + k\left(z_1^{(0)} - z_2^{(0)} + z_{01} - z_{02}\right) - \sigma_0\varepsilon_0 + E_{1\leftrightarrow 2}^H + E\varepsilon_0(z_{01}\varepsilon_c - z_{02}\varepsilon_a) - z_{12}(2k + E\varepsilon_0^2) \quad (3)$$

where x is the displacement of the mass in Fig. 2(b) with respect to its initial displacement. Definitions of other parameters can be found in Table 1. The magnetic energy difference $E_{1\leftrightarrow 2}^H$ between M1 and M2 is calculated as (Chen et al., 2014; Chen and He, 2020):

$$E_{1\leftrightarrow 2}^H = \frac{1}{2}\mu_0 a_2|H|^2 + \langle|H| - \frac{M_S^M}{a_2}\rangle\left(\mu_0 M_S^M|H| - \frac{1}{2}\mu_0 a_2|H|^2 - \frac{1}{2a_2}\mu_0(M_S^M)^2\right) - \frac{1}{2}\mu_0 a_1|H|^2 - \langle|H| - \frac{M_S^M}{a_1}\rangle\left(\mu_0 M_S^M|H| - \frac{1}{2}\mu_0 a_1|H|^2 - \frac{1}{2a_1}\mu_0(M_S^M)^2\right) \quad (4)$$

with $|H|$ being the absolute value of the internal magnetic field strength H, and the function $\langle x\rangle$ being defined as: $\{0,\ \text{if } x < 0;\ 1,\ \text{if } x \ge 0\}$.

According to the material model of martensite reorientation in MSMAs, there are following three cases for the mechanical analysis (Chen and He, 2020). Definitions of all parameters in the following equations can be found in Table 1.

(1) When $|A_{1\leftrightarrow 2}| < \sigma_{tw}^{eff}\varepsilon_0$, with σ_{tw}^{eff} being the effective twinning stress of martensite reorientation estimated as (Chen et al., 2020):

$$\sigma_{tw}^{eff} = \left(0.2 - 0.02 \times (T - A_s^0) \times \left(1 - \tanh\frac{2f_H - 199}{85}\right)\right) \times 10^6 \quad (5)$$

martensite reorientation does not take place. Then we have:

$$m\ddot{x} + c\dot{x} + \left(k_s + E\frac{S}{l_0}\right)x = ES(z_{12}\varepsilon_0 - z_{01}\varepsilon_c + z_{02}\varepsilon_a) \quad (6)$$

(2) When $A_{1\leftrightarrow 2} = \sigma_{tw}^{eff}\varepsilon_0$, M1 switches to M2. Then the volume-fraction transformation z_{12} between M1 and M2 is calculated as:

$$z_{12} = \frac{1}{2k+E\varepsilon_0^2}\left(\frac{E\varepsilon_0}{l_0}x + k\left(z_1^{(0)} - z_2^{(0)} + z_{01} - z_{02}\right) - \sigma_0\varepsilon_0 + E_{1\leftrightarrow 2}^H + E\varepsilon_0(z_{01}\varepsilon_c - z_{02}\varepsilon_a) - \sigma_{tw}^{eff}\varepsilon_0\right) \quad (7a)$$

And the corresponding mechanical equilibrium equation is:

$$m\ddot{x} + c\dot{x} + \left(k_s + \frac{2k}{\varepsilon_0^2}\frac{E}{\left(E+\frac{2k}{\varepsilon_0^2}\right)}\frac{S}{l_0}\right)x = \frac{ES\varepsilon_0}{2k+E\varepsilon_0^2}\left(k\left(z_1^{(0)} - z_2^{(0)} + z_{01} - z_{02}\right) - \sigma_0\varepsilon_0 + E_{1\leftrightarrow 2}^H - \sigma_{tw}^{eff}\varepsilon_0\right) - \frac{2kES}{2k+E\varepsilon_0^2}(z_{01}\varepsilon_c - z_{02}\varepsilon_a) \quad (7b)$$

(3) When $A_{1\leftrightarrow 2} = -\sigma_{tw}^{eff}\varepsilon_0$, M2 switches to M1:

$$z_{12} = \frac{1}{2k+E\varepsilon_0^2}\left(\frac{E\varepsilon_0}{l_0}x + k\left(z_1^{(0)} - z_2^{(0)} + z_{01} - z_{02}\right) - \sigma_0\varepsilon_0 + E_{1\leftrightarrow 2}^H + E\varepsilon_0(z_{01}\varepsilon_c - z_{02}\varepsilon_a) + \sigma_{tw}^{eff}\varepsilon_0\right) \quad (8a)$$

$$m\ddot{x} + c\dot{x} + \left(k_s + \frac{2k}{\varepsilon_0^2}\frac{E}{\left(E+\frac{2k}{\varepsilon_0^2}\right)}\frac{S}{l_0}\right)x = \frac{ES\varepsilon_0}{2k+E\varepsilon_0^2}\left(k\left(z_1^{(0)} - z_2^{(0)} + z_{01} - z_{02}\right) - \sigma_0\varepsilon_0 + E_{1\leftrightarrow 2}^H + \sigma_{tw}^{eff}\varepsilon_0\right) - \frac{2kES}{2k+E\varepsilon_0^2}(z_{01}\varepsilon_c - z_{02}\varepsilon_a) \quad (8b)$$

- Thermal analysis

The temperature evolution due to heat generation and heat convection can be calculated by the following 1D heat equation (Chen and He, 2020):

$$\lambda\dot{T} = (4641.4f_H - 1.35\times 10^5) + \sigma_{tw}^{eff}\varepsilon_0|\dot{z}_{12}| + (A_{01}\dot{z}_{01} + A_{02}\dot{z}_{02} + c_1T(\dot{z}_{01} + \dot{z}_{02})) - \frac{\lambda}{t_h}(T - T_0) \quad (9)$$

where t_h is the characteristic heat relaxation time, which is related to the ambient heat convection coefficient h by: $t_h = \frac{\lambda R}{2h}$. Definitions of other parameters can be found in Table 1. The first three terms on the right-hand-side of Eq. (9) are the heat generation rate due to the eddy current (resulting from the cyclic magnetic field), the intrinsic dissipation of martensite reorientation, and the phase transformation, respectively. The last term on the right-hand-side of Eq. (9) is the rate of heat loss due to the ambient heat transfer. The thermodynamic forces A_{01} and A_{02} in Eq. (9) for the phase transformation are calculated as (Chen and He, 2020):

$$A_{01} = -\frac{E\varepsilon_c}{l_0}x - (k_0 + k + E\varepsilon_c^2)z_{01} - (k_0 - E\varepsilon_a\varepsilon_c)z_{02} + k_0z_0^{(0)} - k\left(z_1^{(0)} - z_{12}\right) + E\varepsilon_0\varepsilon_c z_{12} + \sigma_0\varepsilon_c + (c_0 - c_1T) + E_{01}^H \quad (10a)$$

$$A_{02} = \frac{E\varepsilon_a}{l_0}x - (k_0 - E\varepsilon_a\varepsilon_c)z_{01} - (k_0 + k + E\varepsilon_a^2)z_{02} + k_0 z_0^{(0)} - k\left(z_2^{(0)} + z_{12}\right) - E\varepsilon_0\varepsilon_a z_{12} - \sigma_0\varepsilon_a + (c_0 - c_1 T) + E_{02}^H \quad (10b)$$

with the magnetic energy difference E_{0i}^H (i = 1, 2) between austenite and martensite variant i being:

$$E_{0i}^H = \frac{1}{2}\mu_0 a_i |H|^2 + \langle |H| - \frac{M_S^M}{a_i}\rangle \left(\mu_0 M_S^M |H| - \frac{1}{2}\mu_0 a_i |H|^2 - \frac{1}{2a_i}\mu_0 (M_S^M)^2\right) - \frac{1}{2}\mu_0 a_0 |H|^2 - \langle |H| - \frac{M_S^A}{a_0}\rangle \left(\mu_0 M_S^A |H| - \frac{1}{2}\mu_0 a_0 |H|^2 - \frac{1}{2a_0}\mu_0 (M_S^A)^2\right) \quad (11)$$

With A_{0i} (i = 1, 2) calculated by Eq. (10), we can further calculate the rate $\dot{z}_{0i}$ of the volume-fraction transformation between austenite and martensite variant i as: $\dot{z}_{0i} = LA_{0i}$, where L is a coefficient in the linear kinetics law of phase transformation (Chen and He, 2020). Introducing the value of $\dot{z}_{0i}$ into Eq. (9), the temperature evolution can be obtained.

3. Thermo-magnetic loading effects

The dynamic model in Section 2 is incorporated into the software MATLAB to simulate the behaviour of magnetic shape memory alloys actuated by cyclic magnetic fields under different thermo-magnetic loading conditions. The algorithmic chart is presented in the Appendix. The simulated loading conditions include the ambient heat-transfer condition, the ambient temperature, the applied magnetic field amplitude and frequency, which are studied in detail below.

3.1. Ambient heat-transfer condition

The ambient heat-transfer condition is quantified by the characteristic heat relaxation time t_h: smaller t_h corresponds to stronger ambient heat-transfer condition, and vice versa. Detailed measurement of t_h can be found in (Zhang et al., 2018a, 2020).

Figure 3 shows a typical example of the material's responses to the gradual change of the heat relaxation time t_h. A cyclic magnetic field is applied, as shown in the magnified views in Fig. 3(b). The input magnetic field is a triangular wave changing between +0.78 T and −0.78 T (i.e., with the amplitude of 0.78 T). At the time t_1 (around 200 s), the material's output strain is stabilized, and it is seen from Fig. 3(b) that the output strain is also a triangular wave with the amplitude of 1.81%. The magnified views of the volume fractions (z_1, z_2) of martensite variants at t_1 in Fig. 3(b) reveal the physical mechanism for the strain evolution. When the magnitude of the magnetic field increases (i.e., magnetic loading), the stress-preferred variant M1 switches to the magnetic-field-preferred M2, as shown by the increase in z_2 and the

decrease in z_1 in Fig 3(b), and such variant switching (i.e., martensite reorientation) leads to the strain increase. When the magnitude of the magnetic field decreases (i.e., magnetic unloading), M2 switches back to M1, leading to the strain decrease. Such cyclic martensite reorientation between M1 and M2 results in the cyclic output strain, i.e., strain cyclically changing between a maximum value and a minimum value. And the strain amplitude (i.e., difference between the maximum and the minimum) is almost proportional to the fraction of martensite taking part in the cyclic martensite reorientation, which is represented by the amplitude of the cyclic change in the volume fractions of martensite variants (e.g., 0.31 at t_1 in Fig. 3(b)).

It is also found from the magnified view at t_1 in Fig. 3(b) that the material's response frequency is two times the applied magnetic field frequency. This is because in one cycle of magnetic field, there are two cycles of martensite reorientation: one in the positive magnetic field range (0 ~ 0.78 T) and the other in the negative magnetic field range (−0.78 T ~ 0). Moreover, due to the damping effect of the dynamic system, there is a delay in the material's response: the strain reaches its maximum at a magnetic field magnitude lower than 0.78 T and minimum at a magnetic field magnitude higher than 0 (see t_1 in Fig. 3(b)).

When increasing the heat relaxation time t_h from 1 s to 10 s, the material's stable output strain amplitude increases from 1.81% to 5.85% (see the magnified views of output strain evolution at the times t_1, t_2 and t_3 in Fig. 3(b)) and its stable temperature also increases from 21.20 ℃ to 36.91 ℃ (see Fig. 3(a)). When t_h increases, the ambient heat transfer becomes weaker, so less heat is transferred to the ambient, leading to the increased temperature of the material. With increasing material temperature, the twinning stress (regarded as the frictional stress for martensite reorientation) decreases (see Eq. (5)). In this case, more martensite can take part in the cyclic martensite reorientation process, as shown by the increase in the amplitude of the cyclic change of volume fractions for both variants from 0.31 to 0.99 (see the magnified views at the times t_1, t_2 and t_3 in Fig. 3(b)). Resultantly, the strain amplitude increases.

When the relaxation time t_h continues to increase from 10 s to 80 s, the material's stable output strain amplitude decreases from 5.85% to 0.41% (see the magnified views at the times t_4, t_5 and t_6 in Fig. 3(b)), while its temperature is almost constant around 39 ℃. From the evolution of the volume fraction of austenite in Fig. 3(a), we find that in this range of t_h (> 10 s), the martensite-to-austenite phase transformation is triggered, so the material's temperature stays at the characteristic phase transformation temperature (~ 39 ℃), and the volume fraction of austenite increases from 0 to 0.93 in Fig. 3(a). As a result, less martensite remains in the material to participate in the martensite reorientation, leading to the reduced output strain

amplitude. When t_h is large enough (e.g., 300 s in Fig. 3(a)), the material is fully transformed to austenite, i.e., the volume fraction of austenite is 1. In this case, the material's output strain amplitude is 0, and its temperature (42.63 ℃ in Fig. 3(a)) is higher than the characteristic phase transformation temperature.

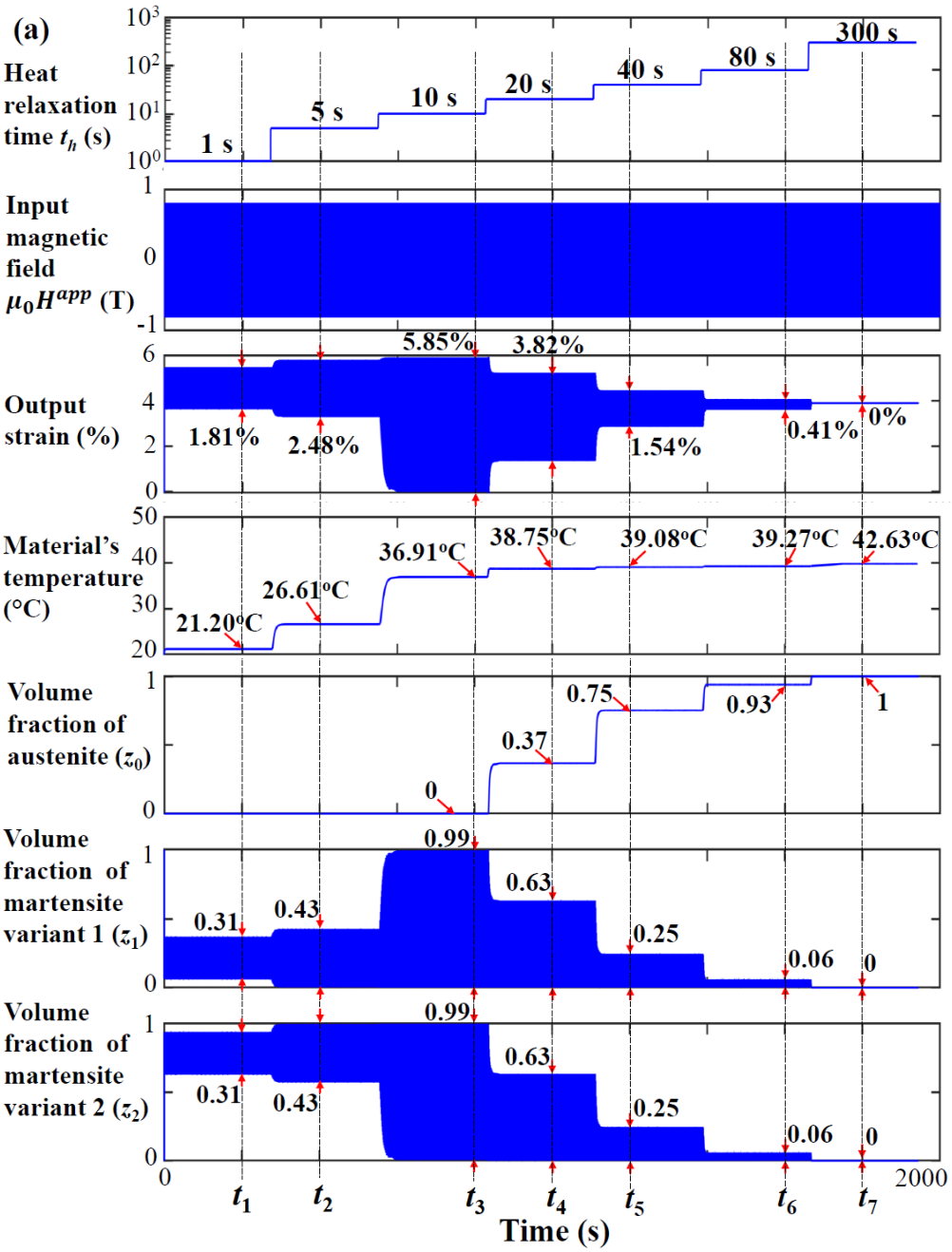

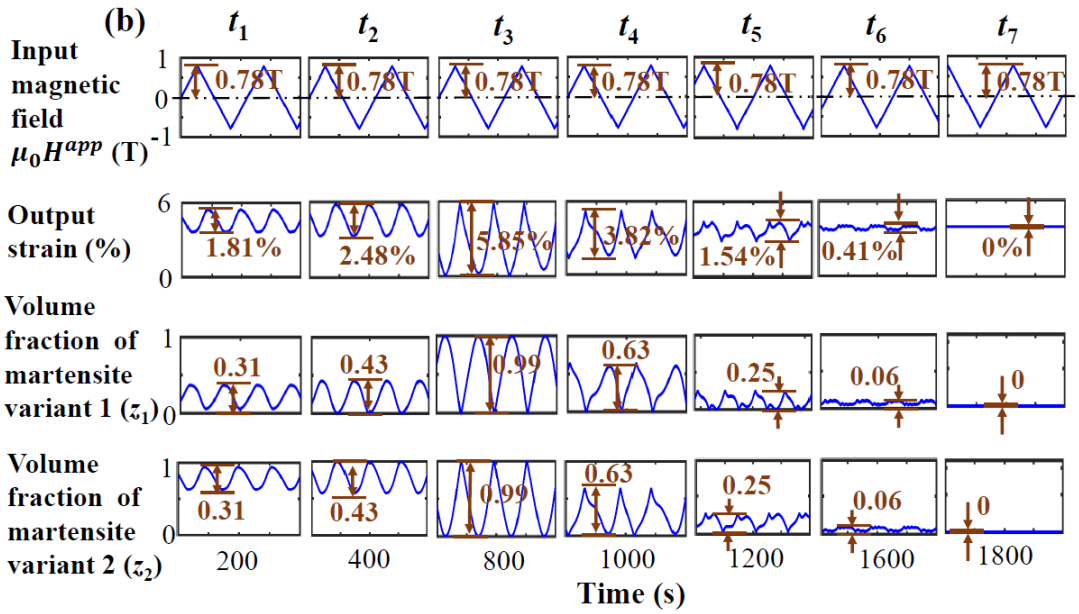

Fig. 3. (a) Material's responses to the gradual change of heat relaxation time t_h. (b) Magnified views of stable states. The span of each view is 0.02 s. The simulation is performed at a magnetic field amplitude of 0.78 T, magnetic field frequency of 90 Hz (so the material's response frequency is $2 \times 90 = 180$ Hz), and ambient temperature of 20 °C.

Figure 4 summarizes the material's stable (i.e., long-term steady state) behaviour at different levels of heat relaxation time t_h. It is seen from the figure that by controlling the value of t_h, the material can exhibit one of following three states:

- $t_h < 12$ s: martensite state (M) with volume fraction of austenite = 0

  In this range of t_h, the ambient heat transfer is strong. So the material's stable temperature is below the characteristic phase transformation temperature (~ 39 °C) and the material is in the martensite state. The output strain amplitude is controlled by the temperature-dependant martensite reorientation process.

- $12 \text{ s} \leq t_h < 270$ s: mixture state (M&A) where martensite and austenite coexist, with volume fraction of austenite between 0 and 1

  The ambient heat transfer is weak in this range of t_h, so the material's stable temperature reaches the characteristic phase transformation temperature, triggering the martensite-to-austenite transformation. In this case, the material contains both austenite and martensite phases, and its output strain amplitude is governed by the temperature-driven phase transformation.

- $t_h \geq 270$ s: austenite state (A) with volume fraction of austenite = 1

In this range, the ambient heat transfer is so weak that the material's stable temperature becomes higher than the characteristic phase transformation temperature. In this case, the material is in the austenite state and its output strain amplitude is 0 since there is no martensite.

The peak of output strain amplitude is found at the boundary between the martensite zone M and the mixture zone M&A. That is because on this boundary, the temperature of the martensite state reaches the maximum, which leads to the minimum twinning stress. So the highest fraction of martensite can take part in the cyclic martensite reorientation, resulting in the largest strain amplitude. Experimental results in the literature are also shown in Fig. 4, and good agreement with model simulations is found.

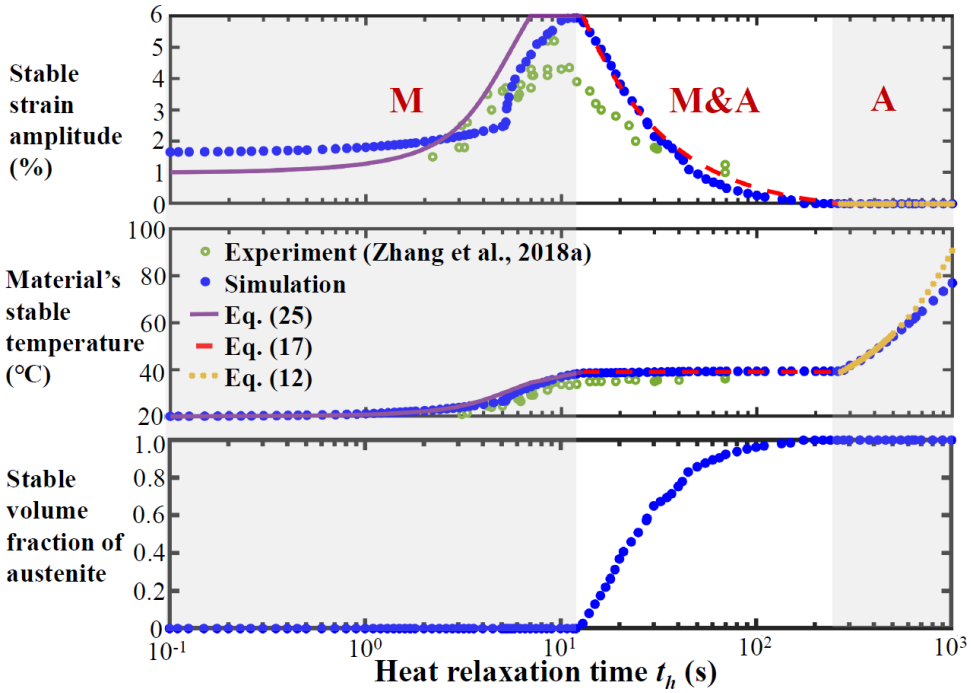

Fig. 4. Material's stable behaviours (i.e., stable output strain amplitude, stable temperature) at different levels of heat relaxation time t_h. Three zones corresponding to three material states are shown: martensite state (M), mixture state (M&A) where martensite and austenite coexist, austenite state (A). All simulations are performed at a magnetic field amplitude of 0.78 T, magnetic field frequency of 90 Hz (so the material's response frequency is $2 \times 90 = 180$ Hz), and ambient temperature of 20 °C.

3.2. Ambient temperature

Figure 5(a) shows a typical example of the material's responses to the gradual change of the ambient temperature T_0. When the ambient temperature is low (e.g., −10 °C in the figure),

the twinning stress is large. In this case, cyclic martensite reorientation cannot be induced. So the material's output strain amplitude is 0 and its stable temperature (e.g., –8.58 °C in the figure) is slightly above the ambient temperature due to the heat from eddy current. When the ambient temperature is increased to 5 °C, the twinning stress is decreased, thus triggering the cyclic martensite reorientation. An increase in the output strain amplitude from 0 to 5.92% is observed in the figure together with an increase in the material's temperature from –8.58 °C to 37.37 °C due to the dissipation heat from cyclic martensite reorientation.

When the ambient temperature is increased further from 5 °C to 30 °C in Fig. 5(a), the material's temperature reaches the characteristic phase transformation temperature (around 39 °C), and the martensite-to-austenite phase transformation is triggered. An increase in the volume fraction of austenite from 0 to 0.79 is observed in Fig. 5(a). Since less martensite remains to take part in the martensite reorientation, the material's output strain amplitude decreases from 5.92% to 1.31%. By further increasing the ambient temperature to 40 °C, the phase transformation is complete, and the material is in the austenite state, i.e., volume fraction of austenite is 1 in Fig. 5(a). The output strain amplitude is 0 in this case since there is no martensite reorientation.

Figure 5(b) summarizes the material's stable behaviour at different levels of ambient temperature T_0. Similar to Fig. 4, the material's state can be controlled by controlling T_0:

- $T_0 < 10$ °C: martensite state (M)
- 10 °C $\leq T_0 < 38$ °C: mixture state (M&A) where martensite and austenite coexist
- $T_0 \geq 38$ °C: austenite state (A)

Moreover, the maximum output strain amplitude is also found near the boundary between the martensite zone M and the mixture zone M&A where the temperature of the martensite state reaches its maximum and the twinning stress reaches its minimum.

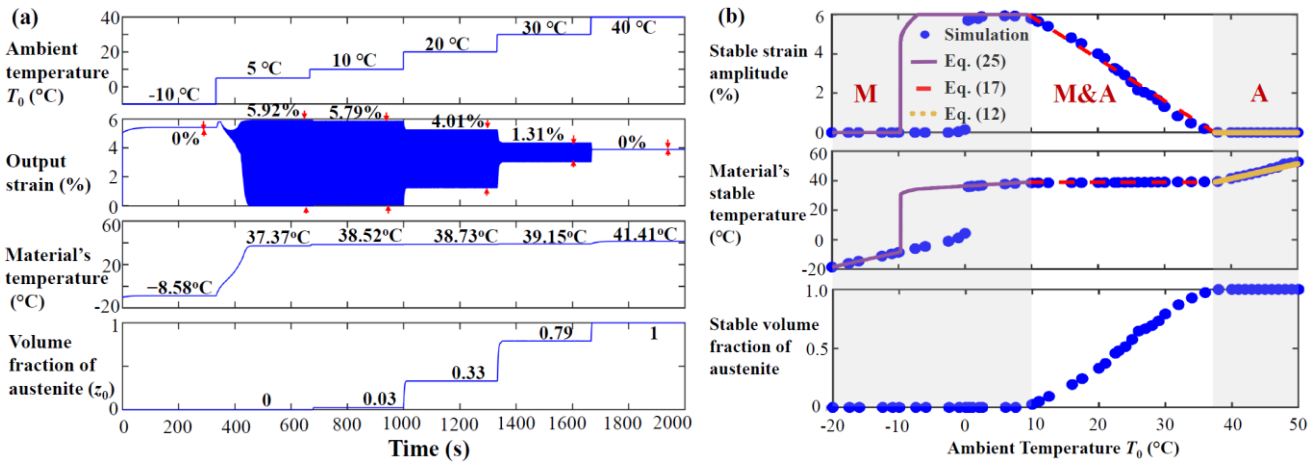

Fig. 5. (a) Material's responses to the gradual change of the ambient temperature T_0. (b) Material's stable behaviours (stable output strain amplitude, stable temperature) at different levels of ambient temperature. Three zones corresponding to three material states are shown: martensite state (M), mixture state (M&A) where martensite and austenite coexist, austenite state (A). All simulations are performed at a magnetic field amplitude of 0.8 T, magnetic field frequency of 90 Hz (so the material's response frequency is $2 \times 90 = 180$ Hz), and heat relaxation time of 20 s.

3.3. Magnetic field amplitude

An example of the material's responses to the gradual change of the applied magnetic field amplitude $\mu_0 H_{amp}^{app}$ is shown in Fig. 6(a). When the magnetic field amplitude is low (e.g., 0.1 T in Fig. 6(a)), the magnetic field cannot induce the switching from the stress-preferred martensite variant M1 (initial state) to the magnetic-field-preferred variant M2. Therefore, the material's output strain remains at 0. By increasing the magnetic field amplitude from 0.1 T to 0.7 T, the M1-to-M2 switching is induced, as shown by the increase in the maximum output strain, and the cyclic martensite reorientation between M1 and M2 is thus triggered. Hence, an increase in the material's output strain amplitude from 0 to 1.82% is observed in Fig. 6(a). At the same time, the material's temperature also increases from 23.16 ℃ to 38.46 ℃ due to the increased dissipation heat from cyclic martensite reorientation. By further increasing the magnetic field amplitude to 1.0 T in Fig. 6(a), the material's stable output strain amplitude increases slightly from 1.82% to 2.19%, and its temperature reaches the characteristic phase transformation temperature (around 39 ℃). In this case, the martensite-to-austenite transformation is triggered, and an increase in the volume fraction of austenite from 0 to 0.64 is observed in Fig. 6(a).

The material's stable behaviour at different levels of applied magnetic field amplitude $\mu_0 H_{amp}^{app}$ is summarized in Fig. 6(b). Depending on the level of $\mu_0 H_{amp}^{app}$, two material states are found:

- $\mu_0 H_{amp}^{app} \leq 0.7$ T: martensite state (M)
- $\mu_0 H_{amp}^{app} > 0.7$ T: mixture state (M&A) where martensite and austenite coexist

It is also found from the figure that in the mixture state (M&A), the applied magnetic field amplitude has little effect on the output strain amplitude. The reason for this will be discussed in Section 4.2.

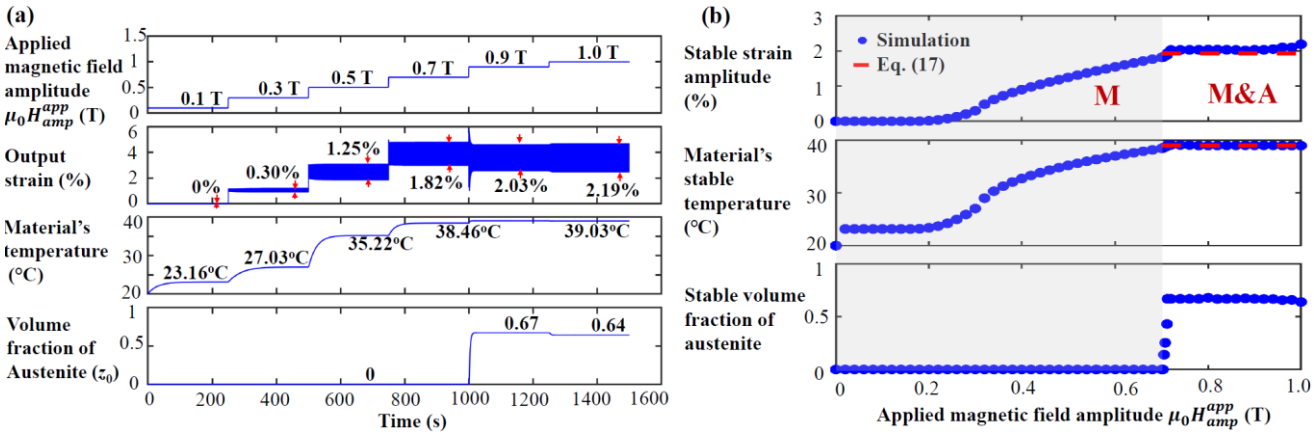

Fig. 6. (a) Material's responses to the gradual change of the applied magnetic field amplitude $\mu_0 H_{amp}^{app}$. (b) Material's stable behaviours (i.e., stable output strain amplitude, stable temperature) at different levels of magnetic field amplitude. Two zones corresponding to two material states are found: martensite state (M), mixture state (M&A) where martensite and austenite coexist. All simulations are performed at a magnetic field frequency of 120 Hz (so the material's response frequency is $2 \times 120 = 240$ Hz), heat relaxation time of 30 s, and ambient temperature of 20 °C.

3.4. Magnetic field frequency

Depending on the ambient thermal conditions, the material can exhibit different frequency responses. In the strong ambient heat-transfer condition and/or low ambient temperature, the material remains in the martensite state, and it exhibits the ordinary resonance-like frequency response (see an example in Fig. 7(b)). By increasing the magnetic field frequency from 50 Hz to 150 Hz in Fig. 7(a), the material's output strain amplitude increases from 3.88% to the peak value of 5.64% at 90 Hz and then decreases to 0.77%. The material's temperature evolution is similar: first it increases to the peak value of 37.68 ℃ at 90 Hz and then decreases to 28.92 ℃. This is because the material's temperature is mainly controlled by the dissipation heat from the cyclic martensite reorientation, which is represented by the output strain amplitude. The material's stable temperature is below the characteristic phase transformation temperature (~ 39 ℃) across the whole simulated frequency range, so the material remains in the martensite state, i.e., the volume fraction of austenite stays at 0 in Fig. 7(a).

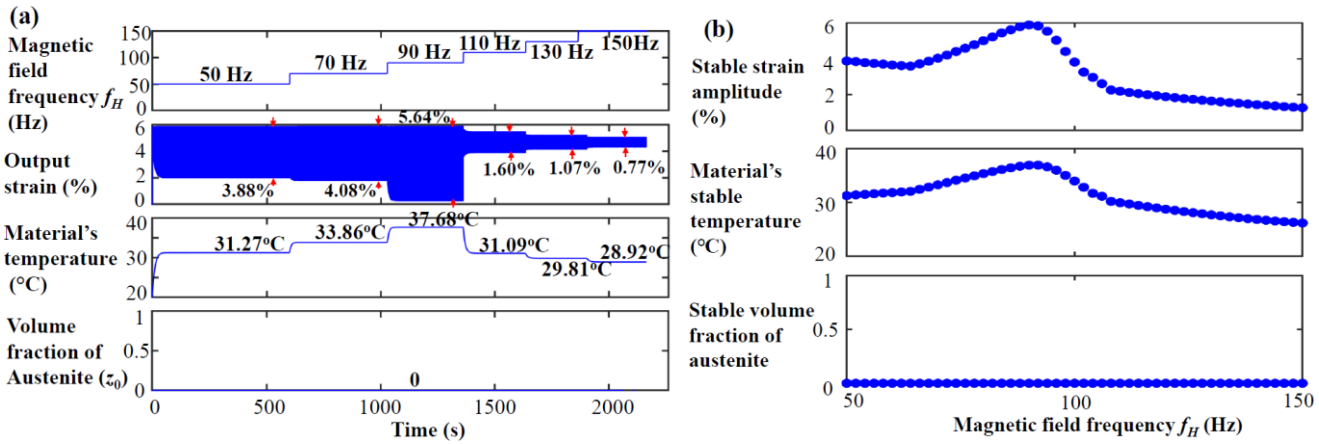

Fig. 7. (a) Material's responses to the gradual change of the magnetic field frequency f_H – I: martensite state. (b) Material's stable behaviours (i.e., stable output strain amplitude, stable temperature) at different levels of magnetic field frequency. All simulations are performed at a magnetic field amplitude of 0.8 T, heat relaxation time of 10 s, and ambient temperature of 20 °C. It is noted that the material's response frequency is two times the applied magnetic field frequency, so the simulated material's response frequency is 100 Hz ~ 300 Hz.

When the ambient heat-transfer condition is weak and/or the ambient temperature is high, the material's temperature can reach the characteristic phase transformation temperature. In this case, the martensite-to-austenite transformation is triggered, and the material is in the mixture state where martensite and austenite coexist. A typical example of the frequency response in this case is shown in Fig. 8(b). Different from the resonance-like frequency response in Fig. 7(b), the strain amplitude decreases monotonically with increasing magnetic field frequency in Fig. 8(b). Detailed material's responses to the gradual change of the magnetic field frequency are shown in Fig. 8(a). It is seen from the figure that when the magnetic field frequency is increased from 50 Hz to 150 Hz, the material's stable output strain amplitude decreases from 2.06% to 0.76%, while its temperature remains around the characteristic phase transformation temperature (~ 39 °C). With increase in the actuation frequency, the accumulation of the dissipation heat from cyclic martensite reorientation becomes quicker, which promotes the martensite-to-austenite transformation. So an increase in the volume fraction of austenite from 0.66 to 0.84 is observed in Fig. 8(a). Since less martensite remains in the material to take part in the martensite reorientation, the output strain amplitude decreases.

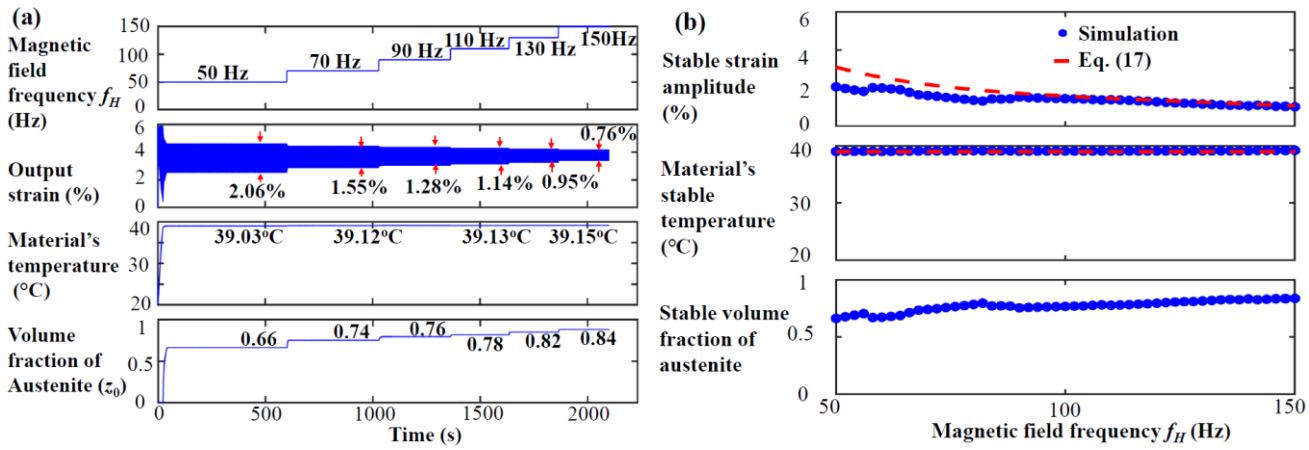

Fig. 8. (a) Material's responses to the gradual change of the magnetic field frequency f_H – II: mixture state. (b) Material's stable behaviours (i.e., stable output strain amplitude, stable temperature) at different levels of magnetic field frequency. All simulations are performed at a magnetic field amplitude of 0.8 T, heat relaxation time of 40 s, and ambient temperature of 20 °C. It is noted that the material's response frequency is two times the applied magnetic field frequency, so the simulated material's response frequency is 100 Hz ~ 300 Hz.

4. Discussions

Model simulations in Section 3 show that the material's stable behaviours (i.e., stable strain amplitude and temperature) are related to its state, which can be controlled by the thermo-magnetic loading conditions. In total three material states are found:

- Austenite state

  In this state, the material's stable temperature is higher than the characteristic phase transformation temperature T_{PT}, and its output strain amplitude is 0 since there is no martensite.

- Mixture state where martensite and austenite coexist

  The material's stable temperature is around T_{PT}, and its stable output strain amplitude can be modulated by the thermo-magnetic loadings.

- Martensite state

  In this state, the material's stable temperature is below T_{PT}. Both its stable temperature and stable output strain amplitude can be modulated by the thermo-magnetic loadings.

Detailed analysis of material's stable (i.e., long-term steady-state) behaviour in these three states is given below. Definitions of all parameters in the following equations can be found in Table 1.

4.1. Austenite state

No martensite reorientation or phase transformation takes place in this state. By neglecting the heat generation terms due to martensite reorientation and phase transformation in the heat equation (Eq. (9)) and further taking $\dot{T} = 0$ (i.e., steady state), we obtain the material's stable temperature as:

$$T_{stable}^{(A)} = T_0 + \frac{t_h}{\lambda}(4641.4 f_H - 1.35 \times 10^5) \tag{12a}$$

The material's stable strain amplitude $\Delta\varepsilon_{stable}^{(A)}$ is 0 since no martensite reorientation takes place in the austenite state:

$$\Delta\varepsilon_{stable}^{(A)} = 0 \tag{12b}$$

It is seen from Eq. (12a) that the material's stable temperature $T_{stable}^{(A)}$ is always higher than the ambient temperature T_0, and the extra temperature (2nd term on the right-hand-side of Eq. (12a)) is due to the heat from the eddy current (induced by the cyclic magnetic field), which is the only heat source in the austenite state. Moreover, the material's stable temperature increases with increasing heat relaxation time t_h due to a weaker ambient heat-transfer condition. With the parameter values in Table 1, Eq. (12) is plotted in Figs. 4 and 5(b), and good agreement with simulations is found.

4.2. Mixture state where martensite and austenite coexist

In the stable state, the phase transformation has already finished, as shown by the constant levels of volume fraction of austenite at times t_4, t_5 and t_6 in Fig. 3(a). By neglecting the heat generation term due to phase transformation in the heat equation (Eq. (9)) and setting $\dot{T} = 0$ (steady state), we have:

$$(4641.4 f_H - 1.35 \times 10^5) + \sigma_{tw}^{eff}\varepsilon_0|\dot{z}_{12}| = \frac{\lambda}{t_h}(T_{stable} - T_0) \tag{13}$$

The terms on the left-hand-side of Eq. (13) represent the heat generation due to eddy current and martensite reorientation, while the right-hand-side is the heat transferred to the ambient. Eq. (13) shows that in the steady state, the generated heat must balance the released heat. Integrating Eq. (13) for one cycle of the material's response ($= 1/2f_H$, since the material's response frequency is two times the applied magnetic field frequency, as shown by the magnetified views in Fig. 3(b)), we have:

$$(4641.4 f_H - 1.35 \times 10^5)\frac{1}{2f_H} + 2\sigma_{tw}^{eff}\varepsilon_0|\Delta z_{12}| = \frac{\lambda}{t_h}(T_{stable} - T_0)\frac{1}{2f_H} \tag{14}$$

where $|\Delta z_{12}|$ is the magnitude of volume fraction change due to cyclic martensite reorientation between M1 and M2. The 2nd term on the left-hand-side of Eq. (14) is multiplied by "2" since

in one cycle, M1 switches to M2 during loading ($+\Delta z_{12}$) and M2 switches back to M1 during unloading ($-\Delta z_{12}$). The material's output strain is mainly due to the martensite reorientation, then we have:

$$\Delta\varepsilon_{stable} \approx \varepsilon_0|\Delta z_{12}| \tag{15}$$

Introducing Eqs. (5) and (15) into Eq. (14), we obtain:

$$\Delta\varepsilon_{stable} = \frac{\frac{\lambda}{t_h}(T_{stable}-T_0)-\left(4641.4f_H-1.35\times10^5\right)}{4f_H\left(0.2-0.02\times\left(T_{stable}-A_S^0\right)\times\left(1-\tanh\frac{2f_H-199}{85}\right)\right)\times10^6} \tag{16}$$

In the mixture state, the material's stable temperature T_{stable} is around the characteristic phase transformation temperature T_{PT}. By taking $T_{stable} = T_{PT}$ in Eq. (16), we obtain:

$$T_{stable}^{(A\&M)} = T_{PT} \tag{17a}$$

$$\Delta\varepsilon_{stable}^{(A\&M)} = \frac{\frac{\lambda}{t_h}(T_{PT}-T_0)-\left(4641.4f_H-1.35\times10^5\right)}{4f_H\left(0.2-0.02\times\left(T_{PT}-A_S^0\right)\times\left(1-\tanh\frac{2f_H-199}{85}\right)\right)\times10^6} \tag{17b}$$

It is found from Eq. (17b) that the stable strain amplitude decreases with increasing heat relaxation time t_h, ambient temperature T_0, and magnetic field frequency f_H. When t_h increases, the ambient heat transfer becomes weaker, so more heat is stored in the material and promotes the martensite-to-austenite transformation. Then less martensite remains to take part in the cyclic martensite reorientation, leading to a reduced output strain magnitude. T_0 and f_H have similar effects. With the increase of f_H, more heat is generated per unit of time due to quicker cyclic martensite reorientation (denominator of Eq. (17b)), so the martensite-to-austenite transformation is pushed forward, leading to less martensite and smaller output strain magnitude. When the ambient temperature T_0 increases, the martensite-to-austenite transformation accelerates, so more martensite is transformed to austenite, resulting in smaller output strain amplitude.

It is also found that Eq. (17b) does not contain the applied magnetic field amplitude $\mu_0 H_{amp}^{app}$, which means $\mu_0 H_{amp}^{app}$ has no effect on the stable strain amplitude. Simulations in Fig. 6(b) also demonstrate minor effect of $\mu_0 H_{amp}^{app}$ in the mixture state. In this state, the strain amplitude depends on the fraction of martensite remaining in the material, which is controlled by the martensite-to-austenite transformation. Since the applied magnetic field ($\leq$ 1 T) is too small to induce phase transformation in MSMAs or significantly change the characteristic phase transformation temperature, it has little effect on the output strain amplitude. Equation (17) is plotted in Figs. 4, 5(b), 6(b), and 8(b), and good agreement is found with both experiments (Fig. 4) and simulations.

The boundary between the mixture state and the austenite state is at: $T_{stable}^{(A)} = T_{stable}^{(A\&M)} = T_{PT}$ and $\Delta\varepsilon_{stable}^{(A)} = \Delta\varepsilon_{stable}^{(A\&M)} = 0$. Both equations lead to:

$$T_0 + \frac{t_h}{\lambda}(4641.4 f_H - 1.35 \times 10^5) = T_{PT} \tag{18}$$

It is seen from Eq. (18) that a high ambient temperature T_0 and a large heat generation due to eddy current (2nd term on the left-hand-side) can drive the material to the austenite state and result in the output strain of 0. To avoid that, we need to reduce the ambient temperature and/or the eddy current heat generation by reducing the magnetic field frequency and/or improving the ambient heat transfer condition (i.e., reducing t_h).

4.3. Martensite state

In contrast to the previous states, where either the material's stable temperature or its stable output stain amplitude is constant, in this state, both temperature and strain amplitude vary with the thermo-magnetic loading conditions. To obtain a stable temperature and stable output strain amplitude, another equation is needed in addition to that derived from the heat equation (Eq. (16)).

Cyclic martensite reorientation between M1 and M2 takes place during magnetic actuation. By setting $z_{01} = z_{02} = 0$ (no phase transformation in the martensite state) and introducing $z_1 = z_1^{(0)} - z_{12}$ and $z_2 = z_2^{(0)} + z_{12}$ in Eq. (3), we obtain the thermodynamic force $A_{1\leftrightarrow 2}$ for martensite reorientation as:

$$A_{1\leftrightarrow 2} = E\varepsilon_0(\varepsilon - z_{12}\varepsilon_0) - \sigma_0\varepsilon_0 + k(z_1 - z_2) + E_{1\leftrightarrow 2}^H \tag{19}$$

During magnetic loading, M1 switches to M2, leading to the increase of output strain. According to the material model of martensite reorientation in MSMAs (Chen et al., 2014), when M1 switches to M2, $A_{1\leftrightarrow 2} = \sigma_{tw}^{eff}\varepsilon_0$. Considering the case when the material's output strain reaches maximum, its velocity is 0 (local maximum), so the damping force (proportional to velocity) is 0. Moreover, since the actuation signal (i.e., input magnetic field) is a triangular wave, the resulted material's response (i.e., output strain) is also an approximately triangular wave as shown by the magnified views at t_1, t_2 and t_3 in Fig. 3(b). In this case, near the maximum strain, the material's acceleration is around 0 (constant slope in the triangular wave), which leads to the zero inertial force. In this special case of zero damping force and zero inertial force, the restoring force f_{MSMA} provided by the material is only balanced by the spring force (see Fig. 2(b)), then we have:

$$f_{MSMA} + f_{spring} = 0$$

$$\longrightarrow ES(\varepsilon_{max} - z_{12}\varepsilon_0) + k_s l_0 \varepsilon_{max} = 0 \longrightarrow E(\varepsilon_{max} - z_{12}\varepsilon_0) = -\frac{k_s l_0}{S}\varepsilon_{max} \quad (20)$$

Introducing Eq. (20) into Eq. (19) and setting $z_1 = 1$ and $z_2 = 0$ (supposing the material is in pure M1 for M1-to-M2 switching), we obtain:

$$A_{1\leftrightarrow 2} = \sigma_{tw}^{eff}\varepsilon_0 \longrightarrow \sigma_{int} - \left(\sigma_0 + \frac{k_s l_0}{S}\varepsilon_{max}\right) + \sigma_H^{(1)} = \sigma_{tw}^{eff} \quad (21)$$

where $\sigma_{int} = \frac{k}{\varepsilon_0}$ and $\sigma_H^{(1)}(= \frac{E_{1\leftrightarrow 2}^H}{\varepsilon_0})$ is the magneto-stress.

In the case when M2 switches back to M1 during magnetic unloading, the output strain decreases and $A_{1\leftrightarrow 2} = -\sigma_{tw}^{eff}\varepsilon_0$. Following similar procedures, we obtain:

$$-\sigma_{int} - \left(\sigma_0 + \frac{k_s l_0}{S}\varepsilon_{min}\right) + \sigma_H^{(2)} = -\sigma_{tw}^{eff} \quad (22)$$

From Eqs. (21), (22), and (5), the output strain amplitude ($= \varepsilon_{max} - \varepsilon_{min}$) can be estimated as:

$$\Delta\varepsilon_{stable} = \frac{S}{k_s l_0}\left(\Delta\sigma_H + 2\sigma_{int} - 2 \times \left(0.2 - 0.02 \times \left(T_{stable} - A_s^0\right) \times \left(1 - \tanh\frac{2f_H - 199}{85}\right)\right) \times 10^6\right) \quad (23)$$

where $\Delta\sigma_H = \sigma_H^{(1)} - \sigma_H^{(2)}$. The magneto-stresses $\sigma_H^{(1)}$ and $\sigma_H^{(2)}$ depend on the magnitude of the applied magnetic field. In the quasi-static case, the strain reaches maximum at the maximum applied magnetic field magnitude of $\mu_0 H_{amp}^{app}$ and minimum at the minimum magnetic field magnitude of 0. But in the dynamic case, due to the damping effect of the dynamic system, there is a delay in the material's response (see Fig. 3(b)), so the strain reaches maximum at a magnetic field magnitude lower than $\mu_0 H_{amp}^{app}$ and minimum at a magnetic field magnitude higher than 0. The phase lag (delay) depends on the magnetic field frequency f_H. Therefore, the magneto-stress difference $\Delta\sigma_H(= \sigma_H^{(1)} - \sigma_H^{(2)})$ is a function of $\mu_0 H_{amp}^{app}$ and f_H.

Equations (16) and (23) form a set of equations for the material's stable temperature and stable strain amplitude. For convenience, the equation solutions are expressed in the dimensionless form (i.e., normalized temperature and strain amplitude) by using the dimensionless numbers defined in Table 2:

- If $\frac{1}{4}A^2 - B < 0$, with *A* and *B* being:

$$A = \frac{2N_3N_4/N_6 - N_4N_5 - 1}{N_4^2/N_6} \quad (24a)$$

$$B = \frac{N_3^2/N_6 - N_3N_5 - N_1 - N_2}{N_4^2/N_6} \quad (24b)$$

there is no real solution to the equation set. This means martensite reorientation is not triggered. Therefore, the material's output strain amplitude is 0, and its temperature can be calculated by Eq. (16) as:

$$\bar{T}_{stable}^{(M)} = N_1 + N_2 \tag{25a}$$

$$\Delta\bar{\varepsilon}_{stable}^{(M)} = 0 \tag{25b}$$

- If $\frac{1}{4}A^2 - B \geq 0$, there is real solution. By accounting for the boundaries of the normalized strain amplitude ($\Delta\bar{\varepsilon}_{stable} \in [0,1]$), we have:

When $\frac{\sqrt{\frac{1}{4}A^2-B}+\frac{1}{2}A-N_1-N_2}{N_3-N_4\left(\sqrt{\frac{1}{4}A^2-B}+\frac{1}{2}A\right)} < 0$:

$$\bar{T}_{stable}^{(M)} = N_1 + N_2 \tag{25c}$$

$$\Delta\bar{\varepsilon}_{stable}^{(M)} = 0 \tag{25d}$$

When $0 \leq \frac{\sqrt{\frac{1}{4}A^2-B}+\frac{1}{2}A-N_1-N_2}{N_3-N_4\left(\sqrt{\frac{1}{4}A^2-B}+\frac{1}{2}A\right)} \leq 1$:

$$\bar{T}_{stable}^{(M)} = \sqrt{\frac{1}{4}A^2 - B} + \frac{1}{2}A \tag{25e}$$

$$\Delta\bar{\varepsilon}_{stable}^{(M)} = \frac{\sqrt{\frac{1}{4}A^2-B}+\frac{1}{2}A-N_1-N_2}{N_3-N_4\left(\sqrt{\frac{1}{4}A^2-B}+\frac{1}{2}A\right)} \tag{25f}$$

When $\frac{\sqrt{\frac{1}{4}A^2-B}+\frac{1}{2}A-N_1-N_2}{N_3-N_4\left(\sqrt{\frac{1}{4}A^2-B}+\frac{1}{2}A\right)} > 1$:

$$\bar{T}_{stable}^{(M)} = \frac{N_1+N_2+N_3}{1+N_4} \tag{25g}$$

$$\Delta\bar{\varepsilon}_{stable}^{(M)} = 1 \tag{25h}$$

The explicit form of $\Delta\sigma_H\left(\mu_0 H_{amp}^{app}, f_H\right)$ is still unknown. But in the case where $\mu_0 H_{amp}^{app}$ and f_H are constant, we can take $\Delta\sigma_H$ as a constant. By taking $\Delta\sigma_H\left(\mu_0 H_{amp}^{app}, f_H\right) = 1.53$ MPa (best fit with the experiments in Fig. 4) and the parameter values in Table 1, Eq. (25) is plotted in Figs. 4 and 5(b) for the varying ambient thermal conditions and constant magnetic loading conditions, i.e., constant $\mu_0 H_{amp}^{app}$ and f_H. Agreement with simulations is found.

The boundary between the martensite state and the mixture state is at: $\bar{T}_{stable}^{(M)} = \bar{T}_{stable}^{(A\&M)} = 1$ and $\Delta\bar{\varepsilon}_{stable}^{(M)} = \Delta\bar{\varepsilon}_{stable}^{(A\&M)}$. The dimensionless stable temperature $\bar{T}_{stable}^{(A\&M)}$ and stable strain amplitude $\Delta\bar{\varepsilon}_{stable}^{(A\&M)}$ in the mixture state can be obtained by normalizing Eq. (17) and using the dimensionless numbers in Table 2:

$$\bar{T}_{stable}^{(A\&M)} = 1 \tag{26a}$$

$$\Delta\bar{\varepsilon}_{stable}^{(A\&M)} = \frac{1 - N_1 - N_2}{N_3 - N_4} \tag{26b}$$

With the aid of Eqs. (25) and (26), we obtain the boundary between the martensite and the mixture states as:

- If $\frac{1}{4}A^2 - B < 0$, with A and B being given in Eq. (24):

$$N_1 + N_2 = 1 \tag{27a}$$

- If $\frac{1}{4}A^2 - B \geq 0$:

$$\text{When } \frac{\sqrt{\frac{1}{4}A^2 - B} + \frac{1}{2}A - N_1 - N_2}{N_3 - N_4\left(\sqrt{\frac{1}{4}A^2 - B} + \frac{1}{2}A\right)} < 0: \;\; N_1 + N_2 = 1 \tag{27b}$$

$$\text{When } 0 \leq \frac{\sqrt{\frac{1}{4}A^2 - B} + \frac{1}{2}A - N_1 - N_2}{N_3 - N_4\left(\sqrt{\frac{1}{4}A^2 - B} + \frac{1}{2}A\right)} \leq 1: \; \sqrt{\frac{1}{4}A^2 - B} + \frac{1}{2}A = 1 \tag{27c}$$

$$\text{When } \frac{\sqrt{\frac{1}{4}A^2 - B} + \frac{1}{2}A - N_1 - N_2}{N_3 - N_4\left(\sqrt{\frac{1}{4}A^2 - B} + \frac{1}{2}A\right)} > 1: \;\; N_1 + N_2 + N_3 - N_4 = 1 \tag{27d}$$

Table 2. Dimensionless parameters

N_1	Normalized ambient temperature	$\frac{T_0}{T_{PT}}$
N_2	Normalized heat from eddy current	$\frac{4641.4 f_H - 1.35\times10^5}{T_{PT}\lambda/t_h}$
N_3	Normalized dissipation due to martensite reorientation at 0 °C	$\frac{4 t_h f_H \varepsilon_0}{T_{PT}\lambda}\left(2\times10^5 + 2\times10^4 \times A_s^0 \times \left(1 - \tanh\frac{2f_H - 199}{85}\right)\right)$
N_4	Dimensionless temperature coefficient for dissipation of martensite reorientation	$8\times10^4 \times \frac{t_h f_H \varepsilon_0}{\lambda}\left(1 - \tanh\frac{2f_H - 199}{85}\right)$
N_5	Normalized total stress including the effect of magnetic field and interaction	$\frac{\Delta\sigma_H\left(\mu_0 H_{amp}^{app}, f_H\right) + \frac{2k}{\varepsilon_0}}{k_s l_0 \varepsilon_0 / S}$
N_6	Normalized spring energy	$\frac{2 f_H k_s l_0 \varepsilon_0^2 / S}{T_{PT}\lambda/t_h}$
$\bar{T}_{stable}$	Normalized material's stable temperature	$\frac{T_{stable}}{T_{PT}}$
$\Delta\bar{\varepsilon}_{stable}$	Normalized material's stable output strain amplitude	$\frac{\Delta\varepsilon_{stable}}{\varepsilon_0}$

5. Conclusions

This paper theoretically studies the effects of thermo-magnetic loading conditions on the long-term (> 100 s, reaching the steady state) high-frequency (> 100 Hz) dynamic behaviour of magnetic shape memory alloys actuated by cyclic magnetic fields. The studied thermo-magnetic loading conditions include: the ambient thermal conditions of ambient temperature and ambient heat-transfer quantified by the characteristic heat relaxation time, and the

magnetic loading conditions of applied magnetic field amplitude and frequency. Main conclusions are summarized below:

(1) The material's stable (i.e., long-term steady-state) temperature is always higher than the ambient temperature due to the heat from eddy current (resulting from the cyclic magnetic field) and the intrinsic dissipation of magnetic-field-induced cyclic martensite reorientation. Such temperature rise can be high enough that the characteristic phase transformation temperature is reached. In this case, the martensite-to-austenite transformation is triggered, and the material is in a mixture state where both martensite and austenite exist. In certain cases, the material's stable temperature can even exceed the phase transformation temperature. Then the phase transformation is complete, and the material is in the austenite state.

(2) The material's stable temperature and state (i.e., martensite, austenite, mixture with coexisting martensite and austenite) can be controlled by the thermo-magnetic loading conditions. Weak ambient heat-transfer, high ambient temperature, and high magnetic field amplitude (to trigger martensite reorientation) lead to large net heat (= generated heat – transferred heat to the ambient) from eddy current and dissipative martensite reorientation, which increases material's stable temperature and can change its state from the initial martensite state to the mixture state and even further to the austenite state.

(3) The material's stable strain amplitude depends on its stable state. In the austenite state, there is no martensite reorientation, so the material's output strain amplitude is 0. In the mixture state, the material's output strain amplitude is controlled by the fraction of martensite remaining in the material, which is related to the temperature-driven martensite-to-austenite transformation. In the martensite state, the material's output strain amplitude is controlled by the fraction of martensite taking part in the cyclic martensite reorientation, which is related to the temperature-dependent twinning stress.

(4) The material's stable strain amplitudes in the martensite and mixture states can be modulated by the thermo-magnetic loading conditions. In the mixture state, weaker ambient heat transfer, higher ambient temperature and higher magnetic field frequency lead to larger net heat generation rate and promote the martensite-to-austenite transformation, which results in less martensite remaining and smaller strain amplitude. While in the martensite state, the material's higher temperature due to weaker heat transfer, higher ambient temperature and larger magnetic field amplitude (to trigger martensite reorientation) results in lower twinning stress and thus larger output strain amplitude.

(5) Analytical expressions of material's stable temperature and stable output strain amplitude as a function of ambient thermal conditions and magnetic loading conditions are derived. They can be used to guide the modulation of the output strain and working temperature of the magnetic shape memory alloy-based actuators with increased reliability.

Appendix. Algorithmic chart

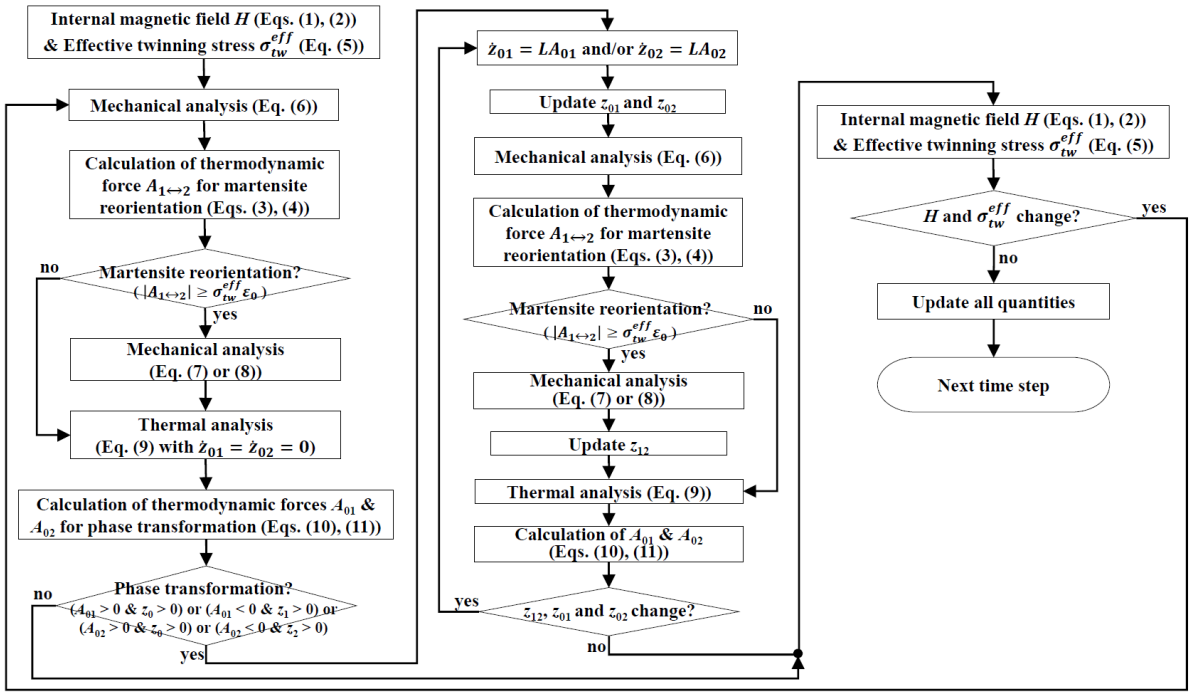

References

Aharoni, A., 1998. Demagnetizing factors for rectangular ferromagnetic prisms. J. Appl. Phys. 83, 3432–3434.

Asua, E., García-Arribas, A., Etxebarria, V. & Feuchtwanger, J. 2014. Pulsed-mode operation and performance of a ferromagnetic shape memory alloy actuator. Smart Mater. and Struct. 23, 025023.

Bastola, A.K., Hossain, M., 2021a. The shape-morphing performance of magnetoactive soft materials performance. Mater. Des. 211, 110172.

Bastola, A.K., Hossain, M., 2021b. Enhanced performance of core-shell hybrid magnetorheological elastomers with nanofillers. Mater. Lett. 297, 129944.

Bruno, N. M., Wang, S., Karaman, I. & Chumlyakov, Y. I. 2016. Reversible martensitic transformation under low magnetic fields in magnetic shape memory alloys. Sci. Rep. 7, 40434.

Chen, X., He, Y. J., 2020. Thermo-magneto-mechanical coupling dynamics of magnetic shape memory alloys. Int. J. Plast. 129, 102686.

Chen, X., He, Y. & Moumni, Z. 2013. Twin boundary motion in NiMnGa single crystals under biaxial compression. Mater. Lt., 90, 72−75.

Chen, X., Moumni, Z., He, Y., Zhang, W., 2014. A three-dimensional model of magneto-mechanical behaviors of martensite reorientation in ferromagnetic shape memory alloys. J. Mech. Phys. Solid. 64, 249–286.

Chernenko, V. A., L'Vov, V. A., Cesari, E. & Barandiaran, J. M. 2019. Chapter 1 - Fundamentals of magnetocaloric effect in magnetic shape memory alloys. In: BRÜCK, E. (ed.) Handbook of Magnetic Materials. Elsevier.

Faran, E. & Shilo, D. 2015. Multi-Scale Dynamics of Twinning in SMA. Shape Memory and Superelasticity, 1, 180−190.

Haldar, K., Lagoudas, D.C., 2018. Dynamic magnetic shape memory alloys responses: Eddy current effect and Joule heating, J. Magn. Magn. Mater. 465, 278–289.

Heczko, O. 2005. Magnetic shape memory effect and magnetization reversal. J. Magn. Mag. Mat., 290-291, 787−794.

Heczko, O., Lanska, N., Soderberg, O. & Ullakko, K. 2002. Temperature variation of structure and magnetic properties of Ni–Mn–Ga magnetic shape memory alloys. J. Magn. Magn. Mat., 242-245, 1446−1449.

Heczko, O., Sozinov, A. & Ullakko, K. 2000. Giant field-induced reversible linear strain in magnetic shape memory NiMnGa alloy. IEEE Trans. on Magn. 36, 3266–3268.

Henry, C.P., 2002. Dynamic Actuation Properties of Ni–Mn–Ga Ferromagnetic Shape Memory Alloys. Ph.D. thesis. Massachusetts Institute of Technology, USA.

Henry, C. P., Bono, D., Feuchtwanger, J., Allen, S. M. & O'Handley, R. C. 2002. ac field-induced actuation of single crystal Ni–Mn–Ga. Am. Ins. Phy. 91, 7810−7811.

Hobza, A., Patrick, C. L., Ullakko, K., Rafla, N., Lindquist, P. & Müllner, P. 2018. Sensing strain with Ni-Mn-Ga. Sens. & Actuators: A. Phy. 269, 137−144.

Karaca, H. E., Karaman, I., Basaran, B., Chumlyakov, Y. I. & Maier, H. J. 2006. Magnetic field and stress induced martensite reorientation in NiMnGa ferromagnetic shape memory alloy single crystals. Acta Mater. 54, 233−245.

Lai, Y.W., Schäfer, R., Schultz, L., McCord, J., 2008. Direct observation of AC field-induced twin-boundary dynamics in bulk NiMnGa. Acta Mater. 56, 5130–5137.

Lindquist, P., Hobza, T., Patrick, L., Mullner, P., 2018. Efficiency of Energy Harvesting in Ni–Mn–Ga Shape Memory Alloys. Shap. Mem. Superelast. 4., 93–101.

Lindquist, P., Müllner, P., 2015. Working Ni–Mn–Ga single crystals in a magnetic field against a spring load. Shap. Mem. Superelast. 1, 69–77.

Lucarni, S., Hossain, M., Gonzalez-Garcia, D., 2022. Recent advances in hard-magnetic soft composites: Syntheses, characterisations, computational modelling, and applications. Compos. Struct. 279, 114800.

Pagounis, E., Chulist, R., Szczerba, M.J., Laufenberg, M., 2014. High-temperature magnetic shape memory actuation in a Ni–Mn–Ga single crystal, Scr. Mater. 83, 29–32.

Pascan, O. Z., He, Y., Moumnia, Z. A. & Zhanga, W. H. 2015. Temperature rise of high-frequency martensite reorientation via Type II twin boundary motion in NiMnGa Ferromagnetic Shape Memory Alloy. Scripta Materialia, 104, 71−74.

Seiner, H., Straka, L., Heczko, O., 2014. A microstructural model of motion of macro-twin interfaces in Ni–Mn–Ga 10M martensite, J. Mech. Phys. Solids. 64, 198–211.

Song, Y., Bhatti, K.P., Srivastava, V., Leighton, C., James, R.D., 2013. Thermodynamics of energy conversion via first order phase transformation in low hysteresis magnetic materials. Energy & Environmental Science 6, 1315−1327.

Sratong-on, P., Chernenko, V. A., Feuchtwanger, J. & Hosoda, H. 2019. Magnetic field-induced rubber-like behavior in Ni-Mn-Ga particles/polymer composite. Sci. Rep. 9, 3443.

Techapiesancharoenkij, R., Kostamo, J., Allen, S.M., O'Handley, R.C., 2009. Frequency response of acoustic-assisted Ni–Mn–Ga ferromagnetic-shape-memory-alloy actuator. J. Appl. Phys. 105, 093923.

Techapiesancharoenkij, R., Kostamo, J., Allen, S.M., O'Handley, R.C., 2011. The effect of magnetic stress and stiffness modulus on resonant characteristics of Ni–Mn–Ga ferromagnetic shape memory alloy actuators. J. Magn. Magn Mater. 323, 3109–3116.

Tickle, R., James, R.D., Shield, T., Wuttig, M., Kokorin, V.V., 1999. Ferromagnetic shape memory in the NiMnGa system. IEEE Trans. Magn. 35, 4301–4310.

Uchimali, M. & Vedantam, S. 2021. Modeling stress–strain response of shape memory alloys during reorientation of self-accommodated martensites with different morphologies. Mech. Adv. Mat. Struc. 1−9.

Ullakko, K., Huang, J. K., Kantner, C., O'Handley, R. C. & Kokorin, V. V. 1996. Large magnetic-field induced strains in Ni2MnGa single crystals. Appl. Phys. Lett. 69, 1966−1968.

Webster, P.J., Ziebeck, K.R.A., Town, S.L., Peak, M.S., 1984. Magnetic order and phase transformation in Ni_2MnGa. Philos. Mag. B 49, 295–310.

Xie, X. 2022. Phase field-finite element analysis of magnetic-induced deformation in ferromagnetic shape memory alloy. Comput. Mater. Sci. 210, 111454.

Yarali, E., Baniasadi, M., Zolfagharian, A., Chavoshi, M., Arefi, F., Hossain, M., Bastola, A., Ansari, M., Foyouzat, A., Dabbagh, A., Ebrahimi, M., Mirzaali, M., Bodaghi, M., 2022. Magneto-/electro-responsive polymers toward manufacturing, characterization, and biomedical/soft robotic applications. Appl. Mater. Today 26, 101306.

Yin, R., Wendler, F., Krevet, B. & Kohl, M. 2016. A magnetic shape memory microactuator with intrinsic position sensing. Sens. & Actuators: A. Phy. 246, 48−57.

Yu, C., Kang, G., Fang, D., 2018. A Thermo-Magneto-Mechanically Coupled Constitutive Model of Magnetic Shape Memory Alloys, Acta Mech. Solida Sin. 31, 535–556.

Zasimchuk, I.K., Kokorin, V.V., Martynov, V.V., Tkachenko, A.V., Chernenko, V.A., 1990. Crystal structure of martensite in Heusler alloy Ni_2MnGa. Phys. Met. Metallogr. 69, 104–108.

Zhang, S., Chen, X., Moumni, Z., He, Y., 2018a. Thermal effects on high-frequency magnetic-field-induced martensite reorientation in ferromagnetic shape memory alloys: an experimental and theoretical investigation. Int. J. Plast. 108, 1–20.

Zhang, S., Chen, X., Moumni, Z., He, Y., 2018b. Coexistence and compatibility of martensite reorientation and phase transformation in high-frequency magnetic-field induced deformation of Ni-Mn-Ga single crystal. Int. J. Plast. 110, 110–122.

Zhang, S., Qin, G., He, Y., 2020. Ambient effects on the output strain of Ni-Mn-Ga single crystal magnetic shape memory alloy. J. Alloys Compd. 835, 155159.